

# Carrier Density-Dependent Localized Surface Plasmon Resonance and Charge Transfer Observed by Controllable Semiconductor

## Content

Xin-Yuan Zhang,<sup>†,‡,§</sup> Donglai Han,<sup>||</sup> Ning Ma,<sup>§</sup> Renxian Gao,<sup>§</sup> Aonan Zhu,<sup>§</sup> Shuang Guo,<sup>§</sup>  
Yongjun Zhang,<sup>§</sup> Yaxin Wang,<sup>§</sup> Jinghai Yang,<sup>\*,§,§</sup> and Lei Chen<sup>\*,§,§</sup>

<sup>†</sup>Changchun Institute of Optics, Fine Mechanics and Physics, Chinese Academy of Sciences, Changchun 130033, PR China

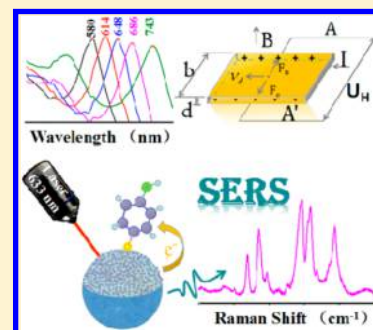
<sup>‡</sup>University of Chinese Academy of Sciences, Beijing 100049, PR China

<sup>§</sup>Key Laboratory of Functional Materials Physics and Chemistry of the Ministry of Education, Jilin Normal University, Changchun 130103, PR China

<sup>||</sup>School of Materials Science and Engineering, Changchun University of Science and Technology, Changchun 130022, PR China

### Supporting Information

**ABSTRACT:** We discuss how the controllable carrier influences the localized surface plasmon resonance (LSPR) and charge transfer (CT) in the same system based on ultraviolet–visible and surface-enhanced Raman scattering (SERS) measurements. The LSPR can be easily tuned from 580 to 743 nm by changing the sputtering power of Cu<sub>2</sub>S in the Ag and Cu<sub>2</sub>S composite substrate. During this process, surprisingly, we find that the LSPR is proportional to the sputtering power of Cu<sub>2</sub>S. This observation indicates that LSPR can be accurately adjusted by changing the content of the semiconductor, or even the carrier density. Moreover, we characterize the carrier density through the detection of the Hall effect to analyze the Raman shift caused by CT and obtain the relationships between them. These fundamental discussions provide a guideline for tunable LSPR and the investigation of CT.



Surface-enhanced Raman scattering (SERS) is an important analytical technique that can be used to perform nondestructive and sensitive detection.<sup>1–4</sup> Usually, the enhancement can be distinguished as being based on the electromagnetic enhancement mechanism (EM) or the chemical enhancement mechanism (CE).<sup>5–8</sup> Localized surface plasmon resonances (LSPRs) are often considered to be primarily based on the EM.<sup>9–11</sup> LSPRs were previously thought to arise only from metallic nanostructures and to be controlled by the size, dielectric environment, shape, and composition of such nanostructures.<sup>12,13</sup> However, recently, many studies demonstrated that LSPRs for semiconductors are of the same status as those for metallic nanostructures.<sup>14–16</sup> The LSPR has been determined to be closely related to the carrier density; as a result, compared with metals, the desired LSPR for semiconductors can be more flexibly adjusted by electronic doping, the creation of intrinsic defects, or the addition of extrinsic impurities.<sup>15,17</sup> CE is a resonance-like process that arises from enhanced polarizability, which reflects the interaction between the adsorbed molecules and the substrate.<sup>18</sup> It is accepted by the community that the primary enhancement modes for CE are (i) ground-state chemical enhancement, which originates from the nonresonant enhancement via the new bond formed between the analyte and the substrate; (ii) resonance Raman enhancement that is caused by surface complexes formed by the analyte and the substrate; and (iii) photon-induced charge-transfer resonance enhance-

ment.<sup>6,19–21</sup> For these three modes, once the incident laser energy matches the band gap, the contribution for charge transfer (CT) will reach the maximum; this phenomenon is analogous to the resonance with the change of incident laser wavelength for LSPR in EM.<sup>22–25</sup>

Clearly, the study of carriers to analyze LSPR and CT for metal–semiconductor composite materials is essential. In recent years, it appears that most researchers have focused only on the CT process between metal and semiconductors in Raman spectroscopy and have paid little attention to their controllable LSPR in the same system.<sup>24</sup> To the best of our knowledge, no similar report exists involving the control of the carrier density by changing the content of the semiconductor in metal–semiconductor composite materials in the investigation of the relationship between LSPR or CT and the carrier density. In this work, we characterized the carrier density using the conventional Hall effect; moreover, we first introduced this method to investigate the Raman shift in Raman spectroscopy. This method facilitates fundamental discussions regarding the relationships among carrier density, LSPR, and CT.

Received: August 6, 2018

Accepted: September 6, 2018

Published: September 6, 2018

A schematic of the fabrication process of the Ag–Cu<sub>2</sub>S composite material is shown in Figure 1. After fabrication of

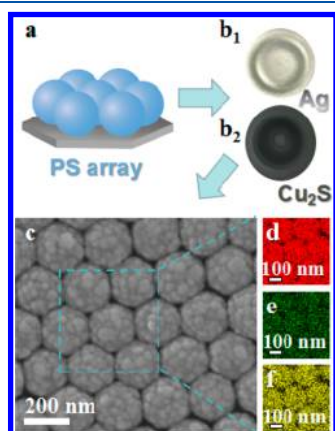


**Figure 1.** Schematic of the preparation of ordered Ag–Cu<sub>2</sub>S array. (a) Two-dimensional ordered polystyrene nanoparticles (PS). (b<sub>1</sub> and b<sub>2</sub>) Optical photographs of the targets. (c) SEM image of the substrate. The power of Ag sputtering is 5 W, and the power for Cu<sub>2</sub>S sputtering is 50 W; the cosputtering time is 30 min. Element maps of (d) Ag, (e) Cu, and (f) S.

two-dimensional ordered monodisperse polystyrene nanoparticle (PS) arrays via self-assembly technology, Ag and Cu<sub>2</sub>S are cosputtered for 30 min. The power of Ag sputtering is 5 W, and the powers for Cu<sub>2</sub>S sputtering are 50, 60, 70, and 80 W for the different compositions of the specimens. The SEM image in Figure 1c shows that the surface of the nanostructure is rough, and element mapping confirmed the uniformity of Ag, Cu, and S. X-ray photoelectron spectroscopy (XPS) results (shown in the Supporting Information) further verified the elements and concentrations.

The absorbance characteristics are illustrated in Figure 2. As shown in Figure 2a, all the absorbance is red-shifted because of the change in content of Cu<sub>2</sub>S. The peaks located on the blue side of 550 nm correspond to the resonance absorbance of Ag,<sup>26,27</sup> and the peaks on the red side are LSPRs for the Ag and Cu<sub>2</sub>S composite.<sup>28,29</sup> With the increase in sputtering power of Cu<sub>2</sub>S, the LSPR is red-shifted from 580 to 686 nm. From a microscopic point of view, this phenomenon corresponds to the significant impact of carrier density on LSPR that causes

the peak to red-shift with the decrease in carrier density.<sup>15</sup> Here, we provide a formula to explain this phenomenon:

$$n_{\text{bulk}} = a\%n_1 + (1 - a\%)n_2 \quad (1)$$

$n_{\text{bulk}}$  is the carrier density of the substrate;  $n_1$  and  $n_2$  are the carrier densities of Ag and Cu<sub>2</sub>S, respectively;  $a\%$  is the ratio of Ag in the substrate. As we know, the carrier density of semiconductors is far less than that of metals. With increasing sputtering power of Cu<sub>2</sub>S, the ratio of Cu<sub>2</sub>S is increased; thus, considering the carriers in the whole system, the decrease in carrier density with increasing Cu<sub>2</sub>S explains the red-shift of the peaks. Moreover, the peak appears to shift regularly with increasing sputtering power. To further analyze the information in the spectra, we provide the linear fitting result between the sputtering power and the maximum absorbance wavelength, given by the red line in Figure 2b. We use  $X$  to represent sputtering power and  $Y$  to represent the maximum absorbance wavelength; the standard curve of the standard solution obeys  $Y = 3.52X + 403.20$ , and  $R^2 = 0.998$ . In other words, in the Ag–Cu<sub>2</sub>S system, when we determine the amount of metal, increasing the ratio of semiconductor will cause the LSPR to red-shift, and the experiment confirmed that the LSPR is proportional to the carrier density.

To investigate the SERS characteristics, *p*-aminothiophenol (PATP) molecules are adsorbed on the surface of substrates. Figure 3a shows the SERS spectra of these substrates recorded using an excitation wavelength of 633 nm. All the band assignments are listed in the Supporting Information. It is obvious that the intensity for a sputtering power of 70 W is the strongest because of the resonant response between the substrate and the laser at an excitation wavelength of 633 nm. Moreover, significant changes appeared in the band at 1389 cm<sup>-1</sup> for sputtering powers of 60 and 70 W; these changes are caused by selective resonant enhancement.<sup>8,19</sup> The peaks located at 1141, 1305, 1389, 1432, and 1575 cm<sup>-1</sup> have been assigned to the b<sub>2</sub> mode of PATP, and all of them appear to shift more or less with changes in the sputtering power.<sup>30–32</sup> Here, we investigated the most remarkable case, i.e., the peak located at 1432 cm<sup>-1</sup>. To analyze the data in detail, we show the enlarged spectrum with a Raman shift from 1350 to 1450 cm<sup>-1</sup> in Figure 3b. The peak located at ~1432 cm<sup>-1</sup> is red-shifted significantly. Generally, Raman shifts are caused by the polarization; in this system, the Raman shift is mainly

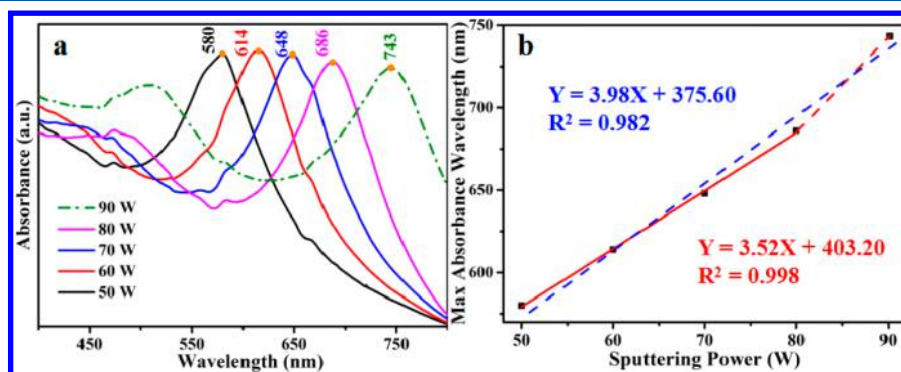


**Figure 2.** (a) Absorbance of the ordered Ag–Cu<sub>2</sub>S array. The line for 50–80 W represents the samples produced by cosputtering Ag and Cu<sub>2</sub>S for 30 min, where the sputtering power of Ag is 5 W and that of Cu<sub>2</sub>S is 50, 60, 70, and 80 W. The dashed line for 90 W represents the sample produced by cosputtering Ag and Cu<sub>2</sub>S for 5 min, where the sputtering power for Ag is 5 W, and that for Cu<sub>2</sub>S is 90 W. (b) Linear fitting result between sputtering power and the maximum absorbance wavelength. The red line is the fit using the data of 50–80 W, and the blue line is the fit using all the data in Figure 2a.

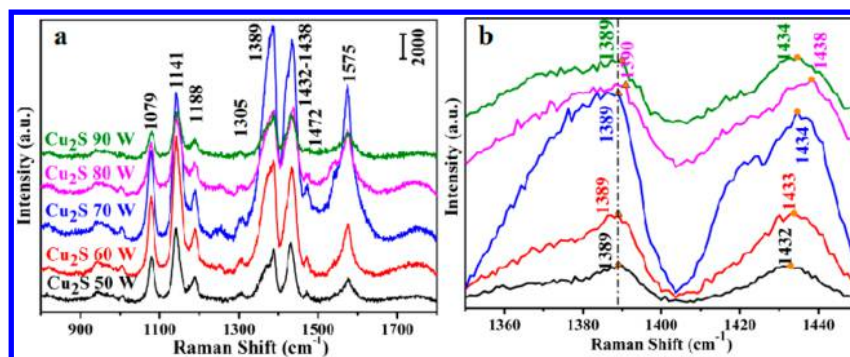


**Figure 3.** (a) SERS spectra of PATP adsorbed on the Ag–Cu<sub>2</sub>S arrays at 633 nm. The line for 50–80 W corresponds to the samples produced by cosputtering Ag and Cu<sub>2</sub>S for 30 min, where the sputtering power for Ag is 5 W, and the sputtering powers for Cu<sub>2</sub>S are 50, 60, 70, and 80 W. The line for 90 W is the sample produced by cosputtering Ag and Cu<sub>2</sub>S for 5 min, where the sputtering power for Ag is 5 W and that for Cu<sub>2</sub>S is 90 W. (b) Enlarged SERS spectra in the spectral range from 1350 to 1450 cm<sup>-1</sup> of Figure 3a.

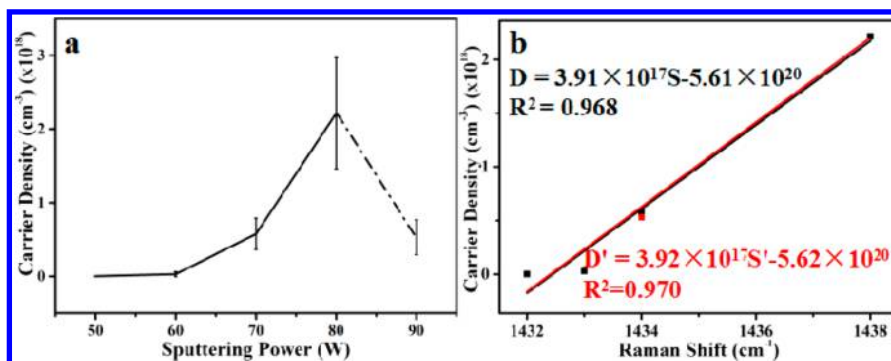


**Figure 4.** (a) Chart of the carrier density for the sample produced by cosputtering Ag and Cu<sub>2</sub>S for 30 min, where the sputtering power for Ag is 5 W and the sputtering powers for Cu<sub>2</sub>S are 50, 60, 70, and 80 W. The point for 90 W is the sample produced by cosputtering Ag and Cu<sub>2</sub>S for 5 min, where the sputtering power for Ag is 5 W and that for Cu<sub>2</sub>S is 90 W. (b) Linear fitting results between Raman shift and carrier density. The black line is the fit to the data of 50–80 W, and the red is the fit to the data of 50–90 W; the red point is the result for the sample produced with a sputtering time of 5 min, with a Cu<sub>2</sub>S sputtering power of 90 W.

attributed to the contribution of Cu<sub>2</sub>S. Here, Cu<sub>2</sub>S is a semiconductor with a narrow band gap (1.2 eV), based on the 633 nm (1.9 eV) laser irradiation; the electrons transfer from the valence band (VB, 5.6 eV) to conduction band (CB, 4.4 eV). The band gap energy between the lowest unoccupied molecular orbital (LUMO) (3.0 eV) of PATP and CB is 1.4 eV, which is lower than the energy of irradiated laser (1.9 eV); then the electrons will transfer from the CB to the LUMO of PATP directly, leading to the reassignment of the electron cloud and the change in polarity.<sup>6,20</sup> As we know, Ag contributes to EM but has little CT; therefore, eq 1 is no longer suitable for investigating the change in carrier density. To quantitatively analyze the influence of Cu<sub>2</sub>S changes on the Raman shift, we first introduce the Hall effect measurement here.

The Hall effect is caused by the combination of electric and magnetic fields and is typically used as a method to detect the carrier density and mobility of semiconductors and metals. Carriers are subjected to opposite forces via the different effects in electric and magnetic fields, resulting in the accumulation of positive and negative charges on opposite planes; using the Hall effect, many basic electrical parameters can be obtained by a simple calculation. In fact, the Hall effect for metals is weaker than that for semiconductors because the resistivity of the material has an essential influence on the Hall effect, i.e., the higher the resistivity is, the easier is the generation of the transverse voltage by Lorentz force, thereby promoting the separation and aggregation of the charge. In the

case in which the Hall effect of Ag is weak and the level is kept the same, we approximate that the influence of the metal is the same in the measured carrier density. Therefore, we can analyze the changes in carriers originating from Cu<sub>2</sub>S in SERS. We analyzed the Hall effect of cosputtered samples with Cu<sub>2</sub>S sputtering powers of 50–80 W. The results are shown in the Supporting Information, and the chart is illustrated in Figure 4a. The carrier density increases with the increase in the Cu<sub>2</sub>S sputtering power. To obtain the effect of carrier density on the CT process, we linearly fit the Raman shift at a position of approximately 1435 cm<sup>-1</sup> (b<sub>2</sub> mode) and the carrier density of these samples, illustrated as the black line in Figure 4b, and found that the standard curve of standard solution obeys  $D = 3.91 \times 10^{17}S - 5.61 \times 10^{20}$ ,  $R^2 = 0.968$ , where  $D$  represents the carrier density and  $S$  represents the Raman shift; the result shows that the two parameters follow a linear relationship. Consequently, for semiconductor systems, the larger the carrier density is, the more significant is the Raman shift.

To further verify the above results, we prepared a sample using a cosputtering time of 5 min, with a sputtering power for Ag of 5 W and that for Cu<sub>2</sub>S of 90 W; the absorbance is shown as the green dashed line in Figure 2a. As illustrated in the figure, the absorbance is further red-shifted to 743 nm; after fitting these data to the samples with a sputtering time of 30 min, which is shown as the blue dashed line in Figure 2b, we found that the standard curve of the standard solution obeys  $Y' = 3.98X' + 375.60$ , and  $R'^2 = 0.982$ . As with the Raman spectra and Hall effect detection results, the results are shown in the

figures, and we fitted all the data collected with a Cu<sub>2</sub>S sputtering power of 50–90 W; the standard curve of the standard solution obeys  $D' = 3.92 \times 10^{17} S' - 5.62 \times 10^{20}$ ,  $R^2 = 0.970$  (red line in Figure 4b). After fitting the results of the sample produced with a cosputtering power of 5 min and a Cu<sub>2</sub>S sputtering power of 90 W, we found that both of the linear solutions still have a linear relationship, indicating that the carrier density is linearly related to both the LSPR and the Raman shift, as described above.

In summary, we reported the results of a study of LSPR and SERS in a metal–semiconductor system. The experimental results showed that, in a certain region, the relationship between carrier density and LSPR remains linear, as does the relationship between carrier density and Raman shift. With the increase in Cu<sub>2</sub>S, the LSPR will red-shift as a result of the decreasing carrier density in the system, and the Raman shift will red-shift because of the increasing carrier density of Cu<sub>2</sub>S. Here, we creatively introduced Hall effect detection to analyze the carrier density in the CT process. The results of this work are expected to pave the way toward further understanding of the effect of carrier density on the LSPR and CT process in SERS.

## ■ ASSOCIATED CONTENT

### Supporting Information

The Supporting Information is available free of charge on the ACS Publications website at DOI: 10.1021/acs.jpcllett.8b02416.

Experimental processes, SEM images, XPS spectra, table for wavenumbers and assignment of bands in SERS of PATP and carrier density and mobility detected by Hall effect (PDF)

## ■ AUTHOR INFORMATION

### Corresponding Authors

\*E-mail: jhyang1@jlnu.edu.cn.

\*E-mail: chenlei@jlnu.edu.cn.

### ORCID

Jinghai Yang: 0000-0001-8409-6035

Lei Chen: 0000-0003-2616-2190

### Notes

The authors declare no competing financial interest.

## ■ ACKNOWLEDGMENTS

This work was supported by the National Natural Science Foundation of China (Nos. 61775081, 61575080, and 61405072) and the Program for the development of Science and Technology of Jilin Province (No. 20150519024JH).

## ■ REFERENCES

- (1) Lombardi, J. R. Raman spectroscopy: Enhanced by organic surfaces. *Nat. Mater.* **2017**, *16*, 878–880.
- (2) Qi, D.; Yan, X.; Wang, L.; Zhang, J. Plasmon-free SERS self-monitoring of catalysis reaction on Au nanoclusters/TiO<sub>2</sub> photonic microarray. *Chem. Commun.* **2015**, *51*, 8813–8816.
- (3) Ji, W.; Song, W.; Tanabe, I.; Wang, Y.; Zhao, B.; Ozaki, Y. Semiconductor-enhanced Raman scattering for highly robust SERS sensing: the case of phosphate analysis. *Chem. Commun.* **2015**, *51*, 7641–7644.
- (4) Chen, L.; Ma, N.; Park, Y.; Jin, S.; Hwang, H.; Jiang, D.; Jung, Y. M. Highly sensitive determination of iron (III) ion based on

phenanthroline probe: Surface-enhanced Raman spectroscopy methods. *Spectrochim. Acta, Part A* **2018**, *197*, 43–46.

- (5) Zhang, X.; Yu, Z.; Ji, W.; Sui, H.; Cong, Q.; Wang, X.; Zhao, B. Charge-Transfer Effect on Surface-Enhanced Raman Scattering (SERS) in an Ordered Ag NPs/4-Mercaptobenzoic Acid/TiO<sub>2</sub> System. *J. Phys. Chem. C* **2015**, *119*, 22439–22444.

- (6) Han, X. X.; Ji, W.; Zhao, B.; Ozaki, Y. Semiconductor-enhanced Raman scattering: active nanomaterials and applications. *Nanoscale* **2017**, *9*, 4847–4861.

- (7) Chen, L.; Sun, H.; Zhao, Y.; Zhang, Y.; Wang, Y.; Liu, Y.; Zhang, X.; Jiang, Y.; Hua, Z.; Yang, J. Plasmonic-induced SERS enhancement of shell-dependent Ag@Cu<sub>2</sub>O core-shell nanoparticles. *RSC Adv.* **2017**, *7*, 16553–16560.

- (8) Zhang, X.-Y.; Han, D.; Pang, Z.; Sun, Y.; Wang, Y.; Zhang, Y.; Yang, J.; Chen, L. Charge Transfer in an Ordered Ag/Cu<sub>2</sub>S/4-MBA System Based on Surface-Enhanced Raman Scattering. *J. Phys. Chem. C* **2018**, *122*, 5599–5605.

- (9) Ding, S. Y.; You, E. M.; Tian, Z. Q.; Moskovits, M. Electromagnetic theories of surface-enhanced Raman spectroscopy. *Chem. Soc. Rev.* **2017**, *46*, 4042–4076.

- (10) Liu, G.; Li, Y.; Duan, G.; Wang, J.; Changhao; Liang; Cai, W. Tunable surface plasmon resonance and strong SERS performances of Au opening-nanoshell ordered arrays. *ACS Appl. Mater. Interfaces* **2012**, *4*, 1–5.

- (11) Xie, W.; Schlucker, S. Surface-enhanced Raman spectroscopic detection of molecular chemo- and plasmocatalysis on noble metal nanoparticles. *Chem. Commun.* **2018**, *54*, 2326–2336.

- (12) Zhou, L.; Tan, Y.; Wang, J.; Xu, W.; Yuan, Y.; Cai, W.; Zhu, S.; Zhu, J. 3D self-assembly of aluminium nanoparticles for plasmon-enhanced solar desalination. *Nat. Photonics* **2016**, *10*, 393–398.

- (13) Hobbs, R. G.; Manfrinato, V. R.; Yang, Y.; Goodman, S. A.; Zhang, L.; Stach, E. A.; Berggren, K. K. High-Energy Surface and Volume Plasmons in Nanopatterned Sub-10 nm Aluminum Nanostructures. *Nano Lett.* **2016**, *16*, 4149–4157.

- (14) Faucheaux, J. A.; Stanton, A. L.; Jain, P. K. Plasmon Resonances of Semiconductor Nanocrystals: Physical Principles and New Opportunities. *J. Phys. Chem. Lett.* **2014**, *5*, 976–985.

- (15) Luther, J. M.; Jain, P. K.; Ewers, T.; Alivisatos, A. P. Localized surface plasmon resonances arising from free carriers in doped quantum dots. *Nat. Mater.* **2011**, *10*, 361–366.

- (16) Liu, N.; Langguth, L.; Weiss, T.; Kastel, J.; Fleischhauer, M.; Pfau, T.; Giessen, H. Plasmonic analogue of electromagnetically induced transparency at the Drude damping limit. *Nat. Mater.* **2009**, *8*, 758–762.

- (17) Li, J. F.; Zhang, Y. J.; Ding, S. Y.; Panneerselvam, R.; Tian, Z. Q. Core-Shell Nanoparticle-Enhanced Raman Spectroscopy. *Chem. Rev.* **2017**, *117*, 5002–5069.

- (18) Yilmaz, M.; Babur, E.; Ozdemir, M.; Gieseck, R. L.; Dede, Y.; Tamer, U.; Schatz, G. C.; Facchetti, A.; Usta, H.; Demirel, G. Nanostructured organic semiconductor films for molecular detection with surface-enhanced Raman spectroscopy. *Nat. Mater.* **2017**, *16*, 918–924.

- (19) Lombardi, J. R.; Birke, R. L. Theory of Surface-Enhanced Raman Scattering in Semiconductors. *J. Phys. Chem. C* **2014**, *118*, 11120–11130.

- (20) Zhang, X.; Liu, Y.; Soltani, M.; Li, P.; Zhao, B.; Cui, B. Probing the Interfacial Charge-Transfer Process of Uniform ALD Semiconductor–Molecule–Metal Models: A SERS Study. *J. Phys. Chem. C* **2017**, *121*, 26939–26948.

- (21) Wang, X.; Li, P.; Han, X. X.; Kitahama, Y.; Zhao, B.; Ozaki, Y. An enhanced degree of charge transfer in dye-sensitized solar cells with a ZnO–TiO<sub>2</sub>/N<sub>3</sub>/Ag structure as revealed by surface-enhanced Raman scattering. *Nanoscale* **2017**, *9*, 15303–15313.

- (22) Ji, W.; Kitahama, Y.; Han, X.; Xue, X.; Ozaki, Y.; Zhao, B. pH-Dependent SERS by Semiconductor-Controlled Charge-Transfer Contribution. *J. Phys. Chem. C* **2012**, *116*, 24829–24836.

- (23) Lum, W.; Bruzas, I.; Gorunmez, Z.; Unser, S.; Beck, T.; Sagle, L. Novel Liposome-Based Surface-Enhanced Raman Spectroscopy (SERS) Substrate. *J. Phys. Chem. Lett.* **2017**, *8*, 2639–2646.

(24) Lombardi, J. R. The theory of surface-enhanced Raman scattering on semiconductor nanoparticles; toward the optimization of SERS sensors. *Faraday Discuss.* **2017**, *205*, 105–120.

(25) Qi, D.; Lu, L.; Wang, L.; Zhang, J. Improved SERS sensitivity on plasmon-free TiO(2) photonic microarray by enhancing light-matter coupling. *J. Am. Chem. Soc.* **2014**, *136*, 9886–9889.

(26) Gong, T.; Zhang, J.; Zhu, Y.; Wang, X.; Zhang, X.; Zhang, J. Optical properties and surface-enhanced Raman scattering of hybrid structures with Ag nanoparticles and graphene. *Carbon* **2016**, *102*, 245–254.

(27) Song, Z. L.; Chen, Z.; Bian, X.; Zhou, L. Y.; Ding, D.; Liang, H.; Zou, Y. X.; Wang, S. S.; Chen, L.; Yang, C.; Zhang, X. B.; Tan, W. Alkyne-functionalized superstable graphitic silver nanoparticles for Raman imaging. *J. Am. Chem. Soc.* **2014**, *136*, 13558–13561.

(28) Ding, X.; Liow, C. H.; Zhang, M.; Huang, R.; Li, C.; Shen, H.; Liu, M.; Zou, Y.; Gao, N.; Zhang, Z.; Li, Y.; Wang, Q.; Li, S.; Jiang, J. Surface plasmon resonance enhanced light absorption and photothermal therapy in the second near-infrared window. *J. Am. Chem. Soc.* **2014**, *136*, 15684–15693.

(29) Liu, Y.; Liu, M.; Swihart, M. T. Plasmonic Copper Sulfide-Based Materials: A Brief Introduction to Their Synthesis, Doping, Alloying, and Applications. *J. Phys. Chem. C* **2017**, *121*, 13435–13447.

(30) Wang, Y.; Ji, W.; Yu, Z.; Li, R.; Wang, X.; Song, W.; Ruan, W.; Zhao, B.; Ozaki, Y. Contribution of hydrogen bonding to charge-transfer induced surface-enhanced Raman scattering of an intermolecular system comprising p-aminothiophenol and benzoic acid. *Phys. Chem. Chem. Phys.* **2014**, *16*, 3153–3161.

(31) Zhang, C.; You, E.; Jin, Q.; Yuan, Y.; Xu, M.; Ding, S.; Yao, J.; Tian, Z. Observing the dynamic "hot spots" on two-dimensional Au nanoparticles monolayer film. *Chem. Commun.* **2017**, *53*, 6788–6791.

(32) Wang, Y.; Yan, C.; Chen, L.; Zhang, Y.; Yang, J. Controllable Charge Transfer in Ag-TiO(2) Composite Structure for SERS Application. *Nanomaterials* **2017**, *7*, 159–169.